

Strengthening of the Riddes Viaduct Through UHPFRC-Based Rehabilitation

Hammad El Jisr Dr, Civil Eng., Lionel Moreillon Dr, Civil Eng. & Philippe Menétrey Dr, Civil Eng.

To cite this article: Hammad El Jisr Dr, Civil Eng., Lionel Moreillon Dr, Civil Eng. & Philippe Menétrey Dr, Civil Eng. (31 May 2023): Strengthening of the Riddes Viaduct Through UHPFRC-Based Rehabilitation, Structural Engineering International, DOI: [10.1080/10168664.2023.2194898](https://doi.org/10.1080/10168664.2023.2194898)

To link to this article: <https://doi.org/10.1080/10168664.2023.2194898>



Published online: 31 May 2023.



Submit your article to this journal [↗](#)



Article views: 77



View related articles [↗](#)



View Crossmark data [↗](#)

Strengthening of the Riddes Viaduct Through UHPFRC-Based Rehabilitation

Hammad El Jisr, Dr, Civil Eng.; Lionel Moreillon, Dr, Civil Eng.; Philippe Menétrey, Dr, Civil Eng., INGPFI, Lausanne, Switzerland.

Contact: hammad.eljisr@ingphi.ch

DOI: 10.1080/10168664.2023.2194898

Abstract

Built in the mid-1970s, the Riddes viaduct is an important viaduct in the Canton of Valais in Switzerland. Thorough inspection of the viaduct revealed structural deterioration of concrete due to alkali–aggregate reaction, as well as corrosion of the prestressing tendons. In an effort to restore the structural integrity of the viaduct, a retrofit intervention that consists of adding a 50 mm layer of an Ultra-High Performance Fibre Reinforced Concrete (UHPFRC) to the deck was proposed. The layer is characterized by its low permeability and excellent mechanical properties. The contribution of the overlay to the load-carrying capacity and stiffness of the viaduct was investigated through a continuum finite element model. Results of the model revealed that the UHPFRC layer significantly enhances the flexural and torsional strength and stiffness of the box girder and ameliorates tensile cracking. The retrofit intervention was deemed beneficial, and the rehabilitation process was carried out.

Keywords: UHPFRC; bridge rehabilitation; structural deterioration; bridge inspection; continuum finite element modelling

Introduction

Highway bridges and viaducts are a class of Reinforced Concrete (RC) structures that are particularly prone to deterioration processes. This is due to their exposure to severe environmental conditions as well as the load modification that occurs over their lifespan. Structural rehabilitation is required to enhance the lifespan of such structures, which can incur significant economic costs. As a result, novel rehabilitation techniques that require minimum intervention have been developed over the past decade.^{1,2} These techniques incorporate Ultra-High Performance Fibre Reinforced Concrete (UHPFRC), characterized by its high compressive (>150 MPa) and tensile (>10 MPa) strength,^{3,4} as well as its extremely low permeability and high resistance to aggressive environmental influences.⁵

Over the past two decades, the implementation of UHPFRC-based bridge rehabilitation has gained traction around the world. In The Netherlands, the orthotropic bridge deck of Van Brienenoord Bridge was reinforced with a 50 mm thick UHPFRC overlay that led to significant stress reduction in the steel deck and the extension of its service life.⁶ Similar rehabilitation techniques have been implemented in Slovenia,⁷

Germany⁸ and Switzerland.⁹ In particular, the strengthening of the Chillon viaduct in Switzerland with a UHPFRC overlay was shown to augment the ultimate resistance of the deck in the transverse direction as well as its flexural stiffness. The overlay also provided a waterproof layer, thereby limiting the progression of Alkali–Aggregate Reactivity (AAR).¹⁰ In the United States, the installation of a UHPFRC overlay was conducted to repair the deteriorated deck of Laporte Road Bridge.¹¹ Other UHPFRC-based rehabilitation techniques included the use of prefabricated UHPFRC elements such as the thin prefabricated slabs that were employed to reinforce the deck of the Grand Pont of Thouaré-sur-Loire in France.¹²

In this article, a real-life rehabilitation of an existing viaduct by means of a UHPFRC layer is presented. The Riddes viaduct is located in the Canton of Valais, Switzerland, and was the subject of severe structural deterioration. The state of the viaduct and damage prior to rehabilitation is first described and assessed, and a retrofit intervention is proposed. A Continuum Finite Element (CFE) model of a portion of the viaduct is then developed to evaluate the contribution of the UHPFRC layer to the response of the deck. In particular, vertical deflections at the serviceability and ultimate limit states are examined. Moreover, the box girder cross-sectional stresses and crack propagation are compared between the initial and UHPFRC reinforced scenarios. Finally, a detailed description of the rehabilitation process is presented.

Description of the Viaduct

The Riddes viaduct, located on the T9 Martigny–Sion cantonal road, crosses the Rhône valley as shown in *Fig. 1*. The general layout and geometry of the viaduct is described by Ref. [13] Referring to *Fig. 2*, the viaduct spans four passages: the SBB Simplon rail line (in orange), the N09 motorway (in green), the plain (in violet) and the river Rhône (in magenta). Four ramps, forming a diamond-shaped junction, connect the viaduct to the N09 motorway platform (see *Figs. 1*



Fig. 1: The Riddes viaduct. Left: location in the Rhône valley. Right: view of the main viaduct near the junction

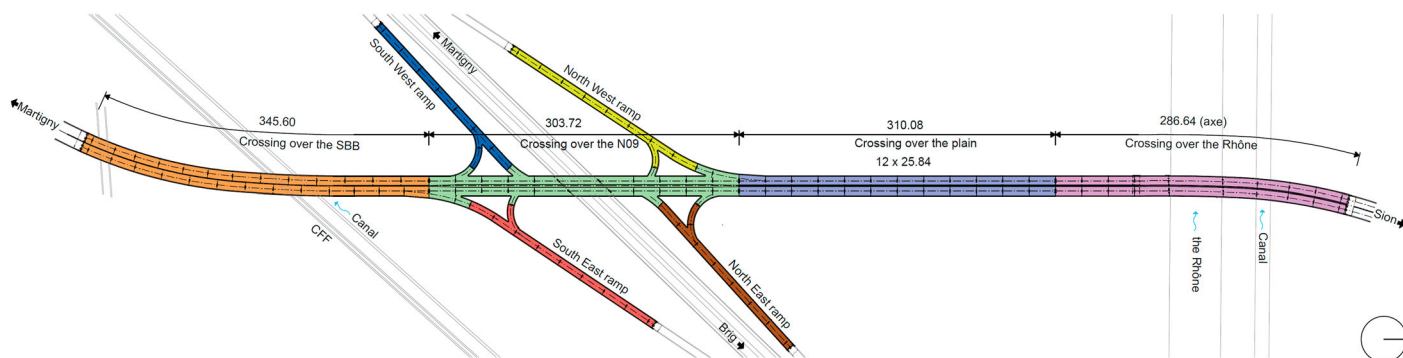


Fig. 2: General layout (plan view) of the viaduct

and 2). The total length of the viaduct, with its ramps and two 1250 m long parallel bridges, is around 3300 m, which makes it one of the longest bridges in the Canton of Valais. The viaduct consists of a multi-span box girder separated into eight sections by means of pavement joints. Typical span lengths range between 24 and 28 m. Over the N09 motorway and the river Rhône, the span lengths increase to 40 and 53 m, respectively.

The deck of the main viaduct is 19.60 m wide and composed of two reinforced and prestressed concrete box girders with a constant height of 1.45 m. Each box girder accommodates two traffic lanes. For the river Rhône section, a variable-height box girder that extends over the adjacent spans above the banks is employed. The deck of the ramps constitutes a box girder as well, whose width is reduced to 8.45 m to accommodate one traffic lane and one shoulder.

In total, the structure is supported by 132 concrete piers. The piers are hexagonal in shape with heights ranging between 5 and 10 m. Each pier is supported on a diaphragm wall with a depth of around 10 m. The piers are connected to the deck through load bearings. A few fixed bearings are utilized at each section of the viaduct to guarantee horizontal stability.

The bridge was designed by Compagnie d'Études et de Réalisations Techniques SA (CERT ingénierie). It is the property of the Swiss Federal Road Office (FEDRO) and the Canton of Valais. The viaduct was put into service in the mid-1970s as part of the Riddes bypass. In the 1990s, major maintenance work was already necessary to replace curbs, waterproofing, pavement, roadway expansion joints and some supporting

structures. In 2018, the INGPHE office was mandated by FEDRO and the Canton of Valais to carry out the upgrading of the structure as part of the "EP Martigny & Environs" project aiming at the rehabilitation of the A9 freeway in Martigny.

Condition of the Viaduct Prior to Intervention

The condition of the viaduct was assessed through visual inspection inside the box girders in accordance with SIA 269.¹⁴ Additionally, both destructive (i.e. concrete core extraction) and non-destructive tests were conducted to evaluate the mechanical and microscopic properties of

concrete, concrete spalling, the chloride content, and the mechanical properties of the steel reinforcement, the prestressing tendons and the encompassing grout. The inspection revealed significant damage in the concrete that rendered the deck prone to water ingress. Damage included cracking and spalling of the concrete cover. In fact, in some spans, cracks were even observed along the path of the prestressing tendons despite the high level of prestress in the box girders. Corrosion of the deck reinforcing bars was also noted. This was accompanied by extensive delamination of concrete in the vicinity of the heavily corroded reinforcement at both the top and bottom flanges (see Fig. 3). Furthermore, the integrity of



Fig. 3: Observed damage inside the box girder of the viaduct. Top right: corrosion of the top flange reinforcement and extensive spalling of concrete. Top left: corroded strands inside a prestressing duct that was opened during inspection. Bottom: spalling of concrete and AAR inside the box girder

the prestressing tendons was assessed at several locations in order to determine the level of corrosion as well as the physical and chemical quality of the injection grout. To that end, the level of alkali–aggregate reactivity was diagnosed both visually and through microscopic and mechanical analyses of the concrete properties. It was shown that corrosion had occurred in four out of six prestressing tendons at certain locations in the web of the box girder as illustrated in Fig. 3, and several tendons were either severed (i.e. actively cut) or slack. The destructive tests revealed that moderate to severe corrosion occurred in 22 out of the 182 drilled holes. Moreover, chloride-contaminated water ingress was detected along the length of some tendons: 65 of the 182 drilled holes showed chloride content in the grout, of which 18 exceeded 0.4% of the weight of cement.

The AAR had developed throughout the whole structure and foundations to a designated pathological level as per Ref. [3]. The tested concrete cores revealed that the elasticity modulus of the concrete had decreased by around 25%. Regarding water infiltration, it was revealed that the water-tightness of the bearing slab was inadequate and that the water drainage system inside the box girders had many defects. These findings were confirmed by the high chloride levels (up to 1.3% of the weight of cement) that were measured in the concrete.

The observed damage in the box girders necessitated a ban on access for heavy traffic over 3.5 tonnes, which was implemented in July 2019.

Proposed Retrofit Intervention

In view of the conducted investigation, a retrofit intervention was deemed necessary in order to restore vital traffic on the bridge and delay the development of the AAR degrading mechanisms. The intervention aimed at optimizing the financial investment for the reduced remaining lifespan of the viaduct. Accordingly, considering the size of the viaduct and to limit the extent of the interventions, traffic on the main viaduct had to be modified by reducing the number of lanes in each direction from two to one. This implied that the right segments over the SBB Simplon rail line, the plain and the river Rhône, which were in a worse condition, should be put out of service as illustrated in Fig. 4.

The main intervention on the preserved decks comprised the installation of a reinforced and waterproof layer of UHPFRC.

The UHPFRC consisted of a fibre content of at least 3% by volume conforming to SIA 2052¹⁵ requirements for class UB-C120. The measured 28-day mean compressive and ultimate tensile strengths were 167 and 14.2 MPa, respectively. Additionally, the consistency test revealed a slump diameter of 500 mm.

The overlay had a theoretical thickness of 50 mm and was cast over the entire length of the deck slab, in accordance with Ref. [1] as well as Ref. [16]. The reinforcing bars in the overlay consisted of B500B Ø12 spaced at 150 mm in both the longitudinal and

transverse directions. The strength enhancement and contribution of the UHPFRC layer to the overall behaviour of the viaduct was examined through a Continuum Finite Element (CFE) model as described in the upcoming section.

Continuum Finite Element Model

Modelling Approach

This CFE model specifics of a section of the Rides viaduct passing over the plain are described herein. This section of the viaduct comprises 12 straight spans, each with a length of 25.84 m. For the sake of computational efficiency, three spans were modelled, and traffic loads were applied on the middle span as illustrated in Fig. 5. The commercial finite element software ANSYS^{®17} was used for this purpose.

Referring to Fig. 5, the deck, piers and UHPFRC layer were meshed with first-order brick elements, SOLID185. Sweep meshing was employed to produce elements with reasonable aspect ratios. Moreover, the mesh was refined in the middle span where traffic loads were applied. For the box girder corresponding to the middle span, four elements per flange/web thickness were employed. On the other hand, the two edge spans were meshed with a coarser mesh. Reinforcing bars in the concrete deck and the UHPFRC layer were modelled using a smeared approach. To account for the effects of prestressing in the deck, the prestressing tendons were modelled

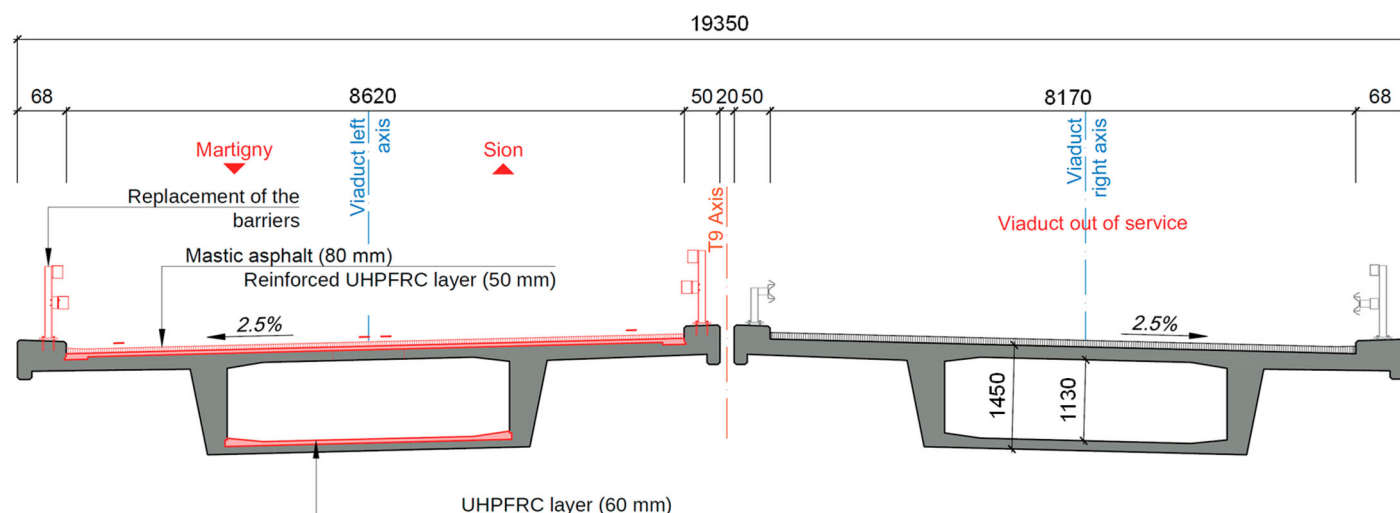


Fig. 4: Left: box girder to which the intervention was implemented. Right: box girder taken out of service

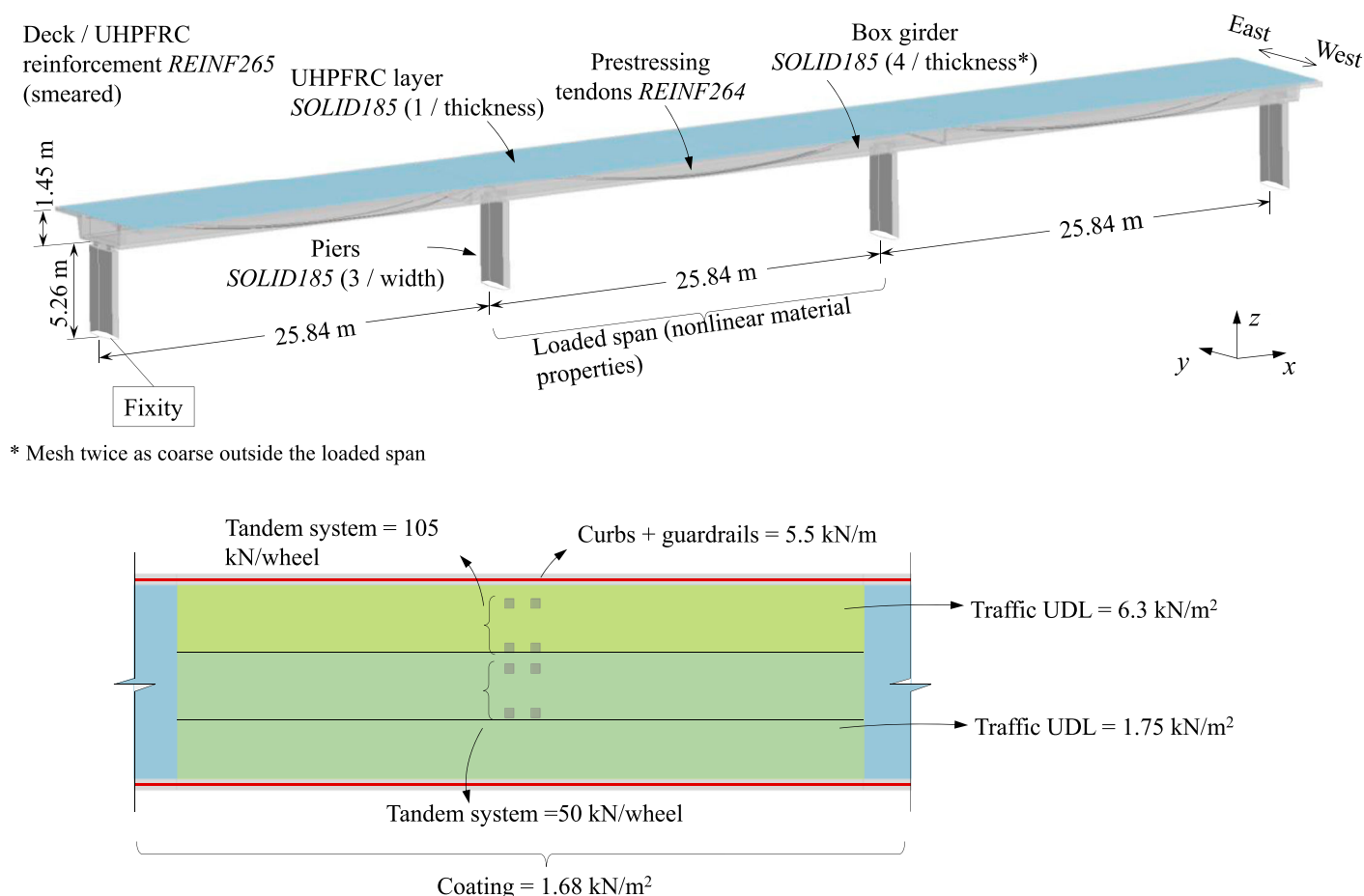


Fig. 5: Continuum finite element model schematic. Top: geometry, element types and boundary conditions. Bottom: applied load on the midspan

using discrete REINF264 elements. Prestressing was applied through an initial strain state that corresponds to 80% σ_0 , where σ_0 is the assumed level of prestress (70% of the yield stress) right after construction was completed in 1976. This assumption is based on past measurements¹⁸ that revealed that prestress losses of up to 20% may occur due to long term creep and shrinkage. Figure 5 shows that fixed boundary conditions were assumed at the base of the piers. The deck was connected to the piers via bearings that allowed rotation in the longitudinal direction while restraining it along the transverse direction.

Material Behaviour

Material nonlinearity was employed in the middle span only. The two edge spans were assigned elastic material properties. The material behaviour of concrete and UHPFRC was simulated through the Menétrey–Willam multi-axial constitutive law¹⁹ available in ANSYS.¹⁷ The model simulates the damage in concrete under a multiaxial stress state. The concrete grade was

C35/45. The mean compressive and tensile strengths of the extracted concrete cores were 55 and 1.85 MPa, respectively. Furthermore, since the tests revealed severe AAR, and in order to account for additional anticipated damage in the 30-year service life, the material properties of the concrete were reduced.¹⁰ These include the modulus of elasticity E_{cm} , which was reduced from 34 to 25 GPa, the characteristic compressive strength f_{ck} , which was reduced to 25 MPa, and the mean tensile strength f_{ctm} , which was reduced to 1 MPa. Since the failure mode of the deck is governed by tensile cracking in the bottom flange of the box girder, it was imperative that the behaviour of concrete under tensile cracking was modelled reasonably well. Hence, the specific fracture energy derived as per fib Model Code 2010²⁰ was reduced to 56 Nm/m² to account for the decrease in the total energy dissipated by fracture as a result of the decrease in the tensile strength of concrete. For UHPFRC, the characteristic material properties in SIA 2052¹⁵ were used. Note that, owing to its

high ductility, the specific fracture energy of UHPFRC is 20,000 Nm/m² as per SIA 2052.¹⁵ A trilinear isotropic material hardening law was applied to the deck reinforcement as well as the prestressing tendons. Furthermore, corrosion in reinforcement that was noted in several regions of the box girder was considered by reducing the yield and ultimate strength of the bars by 10%. While the fibres in the UHPFRC were not modelled explicitly, the enhanced compressive resistance, tensile resistance and ductility of UHPFRC compared to normal strength concrete were accounted for through the material parameters given in SIA 2052.¹⁵ The material properties of the concrete, UHPFRC, deck reinforcement and prestressing tendons are summarized in Table 1.

Degradation Scenarios

The viaduct was analysed under four different scenarios: A, B, AR and BR, as summarized in Table 2. Degradation in concrete and reinforcement was accounted for as described earlier. The corrosion and damage that was

| | Grade | ρ (kg/m ³) | E (GPa) | f_c (MPa) | f_{cb} (MPa) | f_{ct} (MPa) | G_f (Nm/m ²) |
|---------------|--------|-----------------------------|-----------------|------------------|------------------|------------------|----------------------------|
| Concrete | C35/45 | 2400 | 25 ^a | 25 ^a | 29.4 | 1 ^a | 56 |
| UHPFRC | UB | 2400 | 50 | 120 | 129.6 | 12 | 20,000 |
| | Grade | ρ (kg/m ³) | E (GPa) | f_y (MPa) | f_u (MPa) | ϵ_u (%) | G_f (Nm/m ²) |
| Reinforcement | B500B | 7850 | 205 | 450 ^a | 486 ^a | 4.8 | – |
| Tendons | Y1770 | 7850 | 195 | 1520 | 1770 | 2.9 | – |

^aReduced to account for anticipated damage due to AAR and corrosion of reinforcement over the 30-year service life.

ρ = density; E = elastic modulus; f_c = compressive strength of concrete; f_{cb} = biaxial compressive strength as per fib Model Code 2010;²⁰ f_{ct} = tensile strength; G_f = specific fracture energy; f_y = yield strength (0.1% proof yield for the prestressing tendons); f_u = ultimate tensile strength; ϵ_u = strain at ultimate tensile strength.

Table 1: Material parameters used in the continuum finite element model

| Scenario | Prestressing cables | | Deck slab reinforcement |
|----------------------------|--|--|-------------------------|
| | West web | East web | |
| 0: No degradation | 3 × 12T14 $A_p = 4032 \text{ mm}^2$ | 3 × 12T14 $A_p = 4032 \text{ mm}^2$ | No |
| A: Symmetric degradation | $A_p = 2688 \text{ mm}^2$ | $A_p = 2688 \text{ mm}^2$ | No |
| B: Asymmetric degradation | $A_p = 4032 \text{ mm}^2$ | $A_p = 2016 \text{ mm}^2$ | No |
| AR: Symmetric degradation | $A_p = 2688 \text{ mm}^2$ | $A_p = 2688 \text{ mm}^2$ | 50 mm UHPFRC overlay |
| BR: Asymmetric degradation | $A_p = 4032 \text{ mm}^2$ | $A_p = 2016 \text{ mm}^2$ | 50 mm UHPFRC overlay |

Table 2: CFE model analysis scenarios: A, B, AR and BR

detected in the tendons was accounted for by reducing the effective area of the prestressing tendons. Both asymmetric and symmetric degradation scenarios were considered. In scenarios A/AR, the effective area of all prestressing tendons was reduced by a third, whereas scenarios B/BR account for 50% loss in the effective area on the east web of the box girder and the resulting asymmetric response. Note that concrete cracking due to corrosion of failure of prestressing strands was not modelled explicitly. However, the aforementioned reduction in the mechanical properties of concrete can capture the effects of corrosion-induced cracking.

Loading Sequence

The modelled portion of the viaduct was loaded in five stages. A force-controlled method was employed for the analysis. In the first stage, the self-

weight of the viaduct was applied along with the superimposed dead load from the curbs and guard rails (5.5 kN/m). Prestressing of the tendons was implemented at this stage. In the second stage, a uniform load corresponding to the deck coating (1.68 kN/m²) was applied. In the scenarios with reinforcement (AR/BR), the UHPFRC layer, along with its self-weight, were added to the model during this stage. The third and fourth stages constitute the serviceability (rare combination, SLS_{rare}) and ultimate limit states (ULS) according to the load combinations shown in Eqs. (1) and (2), respectively:

$$\text{SLS}_{\text{rare}} = 1.0G + 1.0G_s + 1.0P + 1.0LM1 \quad (1)$$

$$\text{ULS} = 1.15G + 1.15G_s + 1.0P + 1.5LM1 \quad (2)$$

in which G is the self-weight of the viaduct, G_s is the superimposed dead load, P is the prestress, and $LM1$ is the live traffic load corresponding to load model 1 according to SIA 269.¹⁴ The values of the uniform distributed traffic load as well as the tandem system loads are shown in Fig. 5. Finally, in the fifth stage, the middle span was loaded until failure up to 1.5ULS.

Pre-deformations in the deck due to creep and shrinkage were not considered in the model. This is because the concrete deck has experienced severe AAR deterioration, cracking and spalling, and hence the quantification of creep deformation is deemed inaccurate. Moreover, the modulus of elasticity of concrete has been reduced by 30% to account for the deterioration in the concrete. Further reduction in the elastic modulus of concrete to account for creep may lead to an overestimation of the stiffness enhancement due to the addition of UHPFRC reinforcement. Accordingly, it was decided not to reduce the elastic modulus of concrete to account for creep.

Contribution of the UHPFRC Layer to the Behaviour of the Deck

The influence of the UHPFRC layer on the behaviour of the midspan is visible through the load–displacement curves shown in Fig. 6. The load was normalized with that at ULS and the deflection, δ_v , was tracked at midspan. In addition, the vertical displacement of the cantilever wing to which the tandem live load was applied was also tracked. Since non-linear material behaviour was considered in the model, δ_v includes both the elastic and inelastic components.

Referring to Fig. 6, the addition of a UHPFRC layer significantly influences the response, particularly at normalized loads γ_k exceeding 1.0. In the unreinforced scenarios A and B, the run was terminated at $\gamma_k = 1.44$ and 1.46, respectively, owing to excessive plastification in the bottom flange and at the tip of the cantilever wing. Capping of the ultimate load, indicative of the failure load, was observed. On the other hand, both reinforced scenarios attained $\gamma_k = 1.5$. Hence, the load-carrying capacity of the reinforced span is at least 1.5ULS.

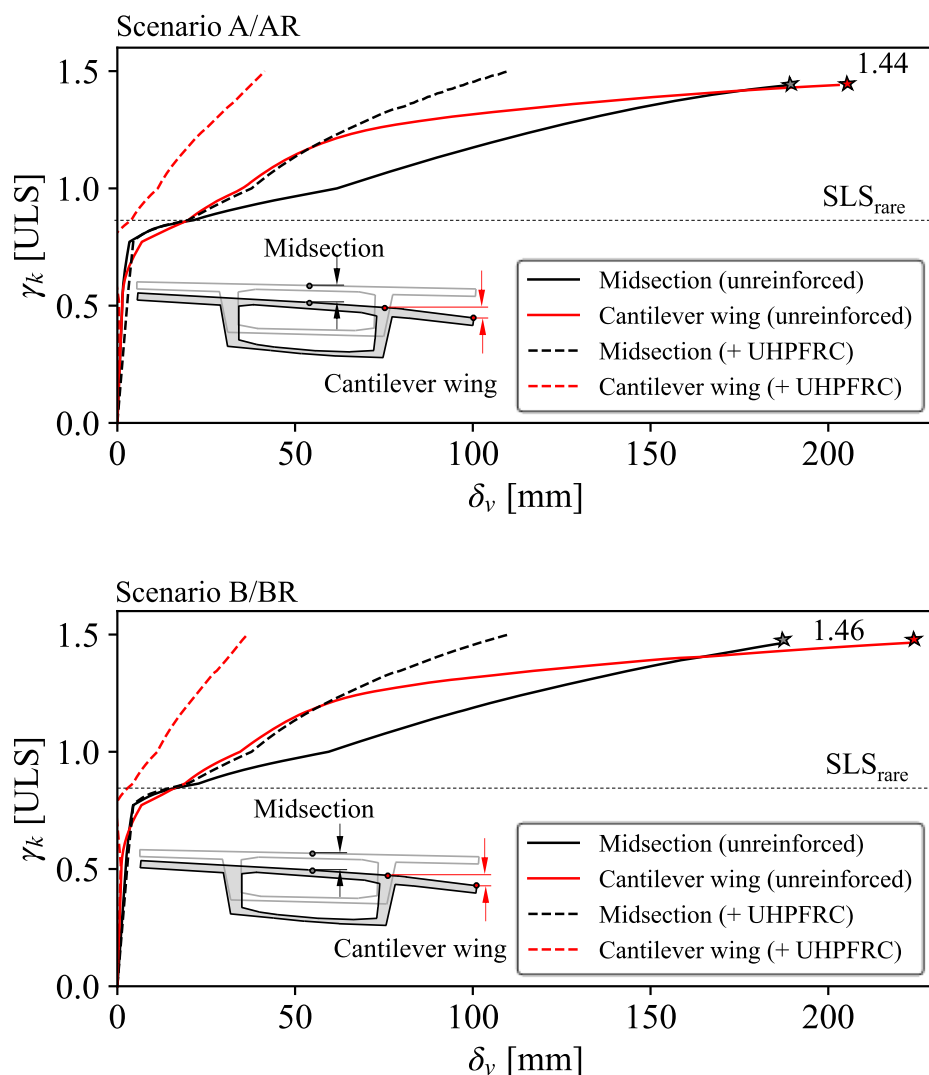


Fig. 6: Normalized load–displacement curves for the different scenarios. Top: symmetric degradation of the prestressing tendons. Bottom: asymmetric degradation of the prestressing tendons

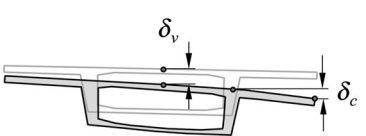
Table 3 shows that, at the midsection, the vertical deflection at the serviceability limit state was reduced by around 15% owing to the addition of the UHPFRC layer. Nonetheless, the deflection was negligible even in the unreinforced scenarios and the span-to-deflection ratio exceeded 1000. The cantilever wing, on the other hand,

experienced large deflections in the unreinforced scenarios: the span-to-deflection ratios were 120 and 126 for scenarios A and B, respectively. This is due to the tensile cracking that occurred at the cantilever support. The addition of the UHPFRC layer enhanced the flexural resistance of the cantilever, thereby delaying the onset

of tensile cracking at the cantilever support. The cantilever deflection significantly decreased by up to six times. Similar behaviour was observed at ULS and at the end of loading, where failure of the cantilever occurred in the unreinforced scenarios.

At the ultimate limit state and beyond, a rapid increase in the deflection at midsection was observed in the unreinforced scenarios as shown in Table 3. This is due to the propagation of tensile cracks from the bottom flange to the web of the box girder. Additionally, the box girder near the piers experienced tensile cracking in its top flange and top part of the web. As such, the flexural rigidity of the box girder diminished at the pier locations leading to excessive span-to-deflection ratios (around 136) at the end of loading. The UHPFRC layer augmented the hogging flexural resistance of the box girder near the piers. This resulted in around a 40% reduction in the deflection at midsection compared to the unreinforced scenarios at ULS and at the end of loading. To illustrate the increase in hogging bending resistance of the box girder at the pier location further, the midsection stresses were traced at SLS_{rare} and ULS at the middle of the north pier.

The mean element stresses along the depth were plotted along the depth of the box girder as shown in Fig. 7. Note that these plots are only indicative since they do not show the stress across the width of the cross section and the stress redistribution that occurs following plastification. Nevertheless, it was observed that, for the unreinforced scenarios (A and B), the stresses in the top flange were low and capped at around 1.0 MPa. The stress distribution was

| | Scenario | Midsection, δ_v (mm) | | | | Cantilever wing, δ_c (mm) | | | |
|--|--------------|--------------------------------|-----|------------------|-----|----------------------------------|----|------------------|----|
| | | A | AR | B | BR | A | AR | B | BR |
|  | SLS_{rare} | 21 | 18 | 23 | 20 | 20 | 3 | 19 | 4 |
| | ULS | 62 | 35 | 59 | 38 | 35 | 9 | 35 | 11 |
| | 1.5 ULS | 190 ^a | 112 | 188 ^b | 110 | 203 ^a | 30 | 223 ^b | 37 |

^aValue at 1.44ULS.
^bValue at 1.46ULS.

Table 3: Vertical displacement values at various levels of loading

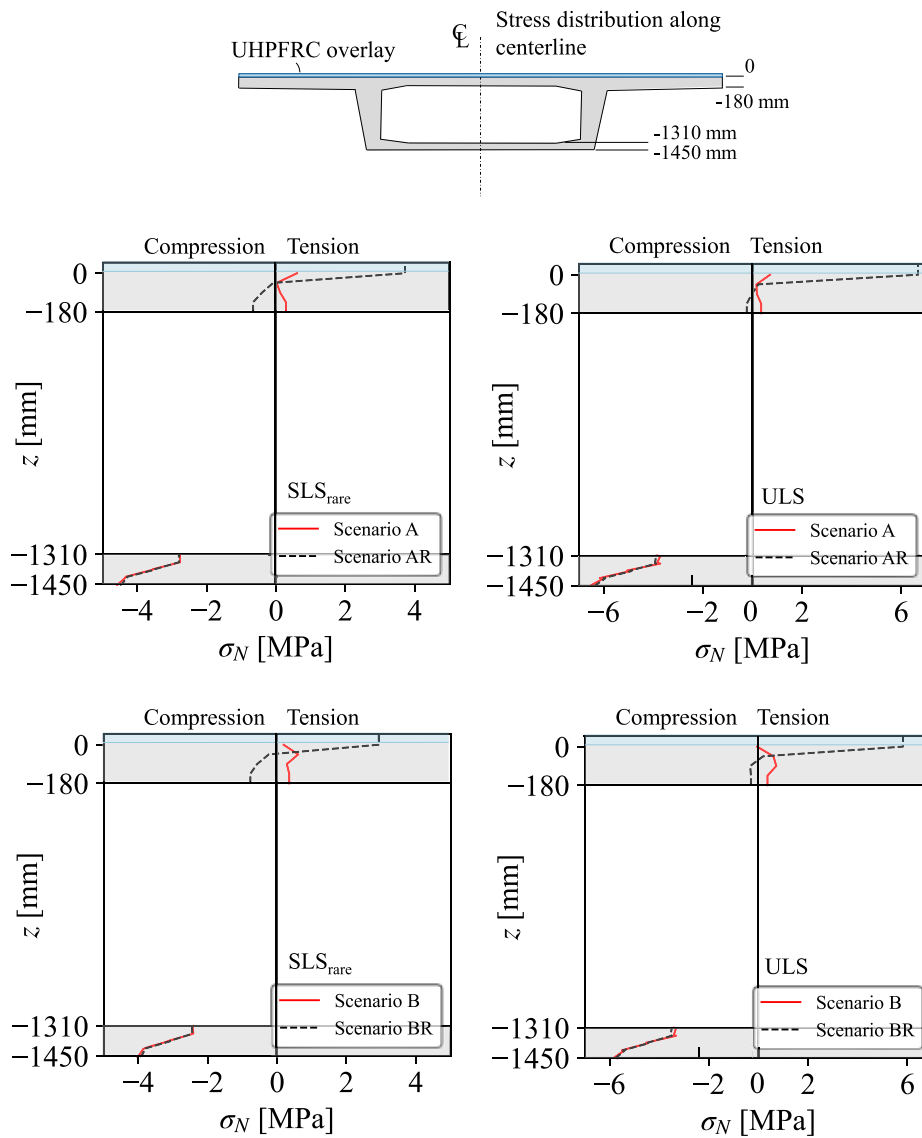


Fig. 7: Stress distribution along the centreline of the box girder section at the North pier. Top left: SLS_{rare} , scenarios A/AR. Top right: ULS, scenarios A/AR. Bottom left: SLS_{rare} , scenarios B/BR; bottom right: ULS, scenarios B/BR

similar at SLS_{rare} and ULS, which indicates capping of the hogging moment. For the reinforced scenarios, the peak tensile stresses were 4 and 3 MPa at SLS_{rare} and 7 and 6 MPa at ULS for scenarios AR and BR, respectively. The cross section was able to resist a higher hogging moment at ULS without any plastification in the UHPFRC layer. Moreover, the addition of the UHPFRC layer shifted the neutral axis upwards, which resulted in a decrease in the tensile stresses and hence tensile cracking in the web. In fact, the web of the box girder was subjected to compressive stresses as shown in Fig. 7.

The crack pattern and crack width were traced at ULS. The latter is

defined by the following equations:²¹

$$d_{cr} = \varepsilon_{p1} \cdot h_{cr} \quad (3)$$

$$h_{cr} = \sqrt[3]{V_e} \quad (4)$$

in which d_{cr} is the crack width, ε_{p1} is the element mean maximum principal plastic strain, h_{cr} is the crack bandwidth and V_e is the element volume.

For brevity, only scenarios A/AR are shown herein. Figure 8 illustrates that, in the unreinforced scenario (A), severe cracking occurred at the edge of the loaded cantilever wing, around the piers and at midspan. The crack widths exceeded 0.3 mm. The crack pattern revealed crack propagation in the top flange around the piers and

towards the web of the box girder. On the other hand, in the reinforced scenario (AR), crack propagation was limited to the bottom region of the box girder at midspan and crack widths were within 0.15 mm. The integrity of the top flange of the box girder (beneath the UHPFRC layer) and the regions in the vicinity of the piers was maintained. This explains the lower deflections observed in the reinforced scenario at ULS compared to the unreinforced scenario, as mentioned earlier. Moreover, in scenario AR with a UHPFRC layer, no tensile cracking occurred in the top flange at the support of the loaded cantilever wing as opposed to the unreinforced scenario. Accordingly, the failure of the cantilever wing that was observed in the unreinforced scenario did not occur.

The finite element analysis revealed that the installation of a 50 mm thick UHPFRC layer on top of the deck augmented both the flexural and torsional stiffness of the midspan, thereby leading to a reduction in the vertical deflections and tensile cracking.

Rehabilitation Process

The viaduct was maintained in an unpropped state during the rehabilitation process. Installation of the reinforcing layer was conducted by first milling and removing the pavement and waterproofing. This was followed by hydrodemolition of the entire wearing surface to a thickness of 20 mm in order to remove the damaged concrete and create a rough surface for bonding the UHPFRC. Near the curbs, grooves were made to bond the UHPFRC layer to the existing reinforcement. The UHPFRC was laid by hand and directed towards grooves made in the deck slab (see Fig. 9).

To complete the retrofit process of the viaduct, the pavement and pavement drainage system were reconstructed. Mastic Asphalt (MA) with an average thickness of 80 mm was applied directly on top of the UHPFRC layers on the viaduct and ramps after treating the surface with very-high-pressure water jets. Furthermore, the inside surface of the bottom flange of the box girders, which showed severe degradation, was retrofitted with a 60 mm thick layer of

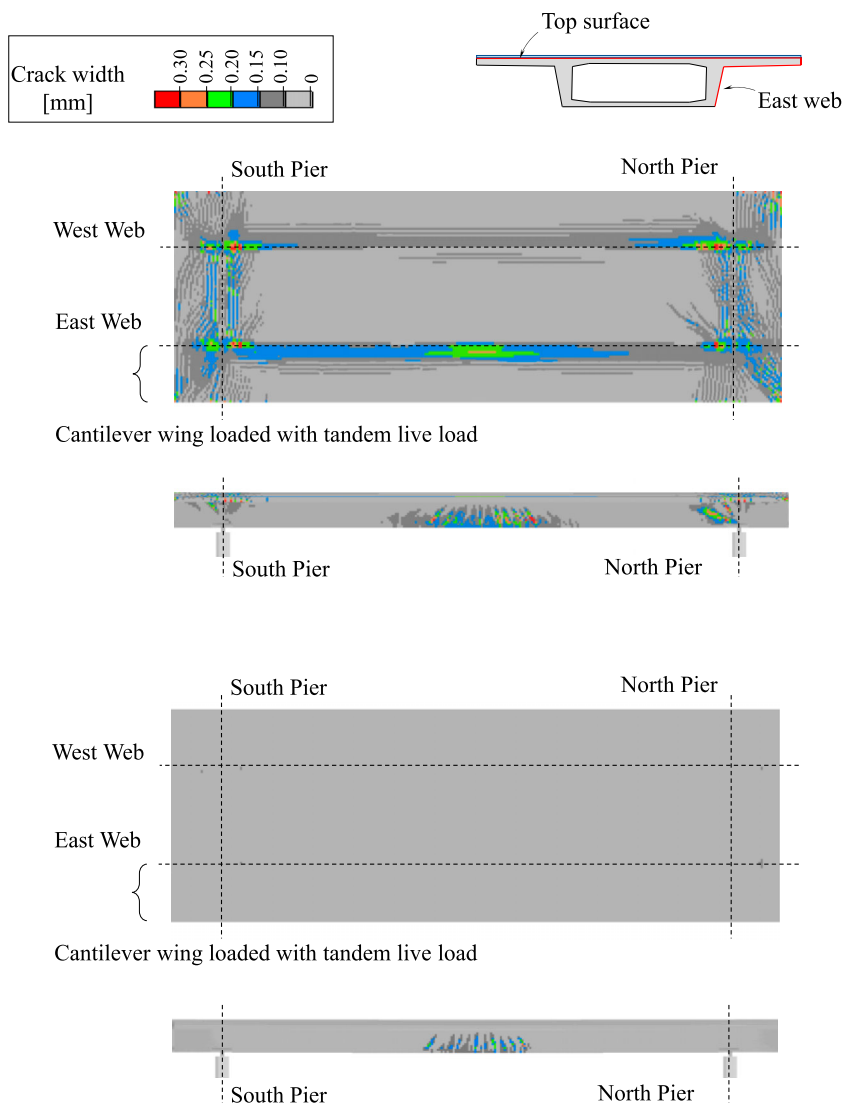


Fig. 8: Crack pattern at ULS: comparison between the (top) original section, scenario A and (bottom) section with UHPFRC overlay, scenario AR



Fig. 9: Retrofit intervention in the Riddes viaduct. Top: installation of the UHPFRC layer on the deck (© Adrien Pilet, reproduced with permission). Bottom left: installation of the UHPFRC layer inside the box girder. Bottom right: application of MA on top of the UHPFRC layer on the deck slab

reinforced UHPFRC. These repairs were deemed necessary to enhance the flexural resistance of the box girder sections under sagging and hogging bending, as well as the stiffness of the deck slab. The intervention also provides waterproofing of the concrete to limit the further development of AAR.¹⁰

Additional reinforcement was provided as part of the retrofitting process. The edge spans of the ramps at each end were longitudinally reinforced under bending by means of PFRC laminates bonded to the underside of the bottom flange. Moreover, the spans of the viaduct that connect the ramps to the N09 motorway were overloaded and hence critical in terms of flexural strength. At three particular regions, additional external prestressing was implemented to compensate for losses in the prestressing tendons due to corrosion. The external prestressing consisted of a seven-stranded cable attached inside the box girder along a trapezoidal path.

Conclusions

This article provides an example of the use of UHPFRC for strengthening large scale structures that have been subject to severe degradation, and the methodology employed to numerically simulate the damage and retrofit intervention. The study was conducted on the Riddes viaduct in the Canton of Valais in Switzerland. The viaduct was first thoroughly inspected to assess the structural deterioration, and a retrofit intervention that mainly involved a 50 mm UHPFRC overlay was proposed. The contribution of the UHPFRC to the performance of the viaduct was then assessed by means of a CFE model. There follows a summary of the main observations and findings.

- Visual inspection and accompanying non-destructive and destructive tests revealed that the deterioration of concrete due to AAR had reached a pathological level. Chloride-contaminated water ingress was detected along the tendons. Moreover, moderate to severe corrosion was identified in several prestressing tendons with some either severed or slack. The deterioration of the deck had progressed to the point where maintenance action was necessary in order

not to reduce the service life and service load of the viaduct.

- The addition of a UHPFRC layer increased the ultimate flexural resistance of the deck by at least 50% of the capacity at ULS. The simulations showed that the unreinforced deck experienced severe cracking in the bottom flange and at the tip of the cantilever wing at ULS, leading to failure at 1.45ULS. On the other hand, minimum damage in the deck was observed in the UHPFRC-reinforced scenarios.
- From a serviceability perspective, the installation of the UHPFRC layer on top of the deck enhanced the flexural and torsional stiffness of the viaduct. Prior to reinforcement, performance under service loads was not compliant with the requirements of SIA 260.²² Excessive deflection occurred at the tip of the cantilever (span-to-deflection ratio lower than 130). The UHPFRC layer led to a reduction of the cantilever deflection by up to six times. Similarly, at the midsection, the vertical deflections were reduced by 40% at ultimate limit state.
- The tensile stresses in the UHPFRC layer were found to be three to seven times higher than those in the top flange of the unreinforced box girder resulting in an upward shift in the neutral axis and a higher hogging bending resistance near the piers.
- Severe cracking was observed at ultimate limit state in the unreinforced scenarios (crack widths greater than 0.3 mm) compared to the reinforced scenarios in which crack propagation was limited to the bottom region of the box girder at midspan (crack widths less than 0.15 mm). Furthermore, the integrity of the top flange of the box girder (beneath the UHPFRC layer) and the regions in the vicinity of the piers was maintained in the reinforced scenarios. The alleviation of flexural cracking of the deck not only reduced water infiltration, but also enhanced the flexural stiffness of the deck, and hence also the lower midsection deflections at ULS.

The rehabilitation process described in the article was completed in less than a year, making it possible to reopen the viaduct to heavy traffic in December 2021. This feat, despite the extent of the damage, was made possible thanks to the mastery of the technical

solutions by all the stakeholders. Nevertheless, to manage the risks, the operation of the viaduct is conditional on the implementation of specific structural health monitoring systems. The article demonstrates the significant benefits that UHPFRC retrofitting provides while being both time and cost efficient. These advantages necessitate the development of a systematic procedure for UHPFRC intervention in order to facilitate and encourage its implementation by practising structural engineers.

Acknowledgements

The authors would like to sincerely thank the Swiss Federal Road Office (FEDRO) and the Canton of Valais for providing the project-related documents. The authors also gratefully acknowledge the assistance of Prof. Brühwiler for his valuable advice as well as the considerable assistance of Mr Francisco Pires in building the finite element model of the viaduct.

Disclosure Statement

No potential conflict of interest was reported by the author(s).

Data Availability Statement

The nonlinear finite element models for the four scenarios considered have been made publicly available in an online repository (10.5281/zenodo.7622118).

References

- [1] Brühwiler E, Denarié E. Rehabilitation and strengthening of concrete structures using ultra-high performance fibre reinforced concrete. *Struct Eng Int*. 2013;23:450–457.
- [2] Denarié E, Brühwiler E. Structural rehabilitations with ultra-high performance fibre reinforced concretes (UHPFRC)/strukturelle Instandsetzung von betonbrücken mit ultra-hochleistungsfähigem faserfeinkornbeton (UHFB). *Res Build Mon*. 2006;12:93–108.
- [3] Denarié E, Brühwiler E. Strain-hardening ultra-high performance fibre reinforced concrete: deformability versus strength optimization. *Res Build Mon*. 2011;17:397–410.
- [4] Wuest J. Structural behaviour in tension of ultra-high performance fibre reinforced concrete in composite elements. PhD Thesis. EPFL, 2007.
- [5] Charron J-P, Denarié E, Brühwiler E. Permeability of ultra high performance fiber reinforced concretes (UHPFRC) under high stresses. *Mater Struct*. 2007;40:269–277.
- [6] Buitelaar P, Braam R, Kaptijn N. Reinforced high performance concrete overlay system for rehabilitation and strengthening of orthotropic

steel bridge decks, Sacramento, USA: Delft University of Technology; 2004, p. 384–401.

- [7] Sajna A, Denarié E, Bras V. Assessment of UHPFRC based bridge rehabilitation in Slovenia, Two years after application. 3rd international Symposium on Ultra-High Performance Concrete, Kassel, Germany; 2012.
- [8] Pelke E, Jaborek A, Berger D, Bruehwiler E. Overpass bridge of the L3378 road near Fulda-Lehnerz First application of UHPFRC in road bridge construction in Germany. *Part 1. Beton-Und Stahlbetonbau* 2018;113:831–841.
- [9] Graybeal B, Brühwiler E, Kim B-S, Toutlemonde F, Voo YL, Zaghi A. International perspective on UHPC in bridge engineering. *J Bridge Eng*. 2020;25(11).
- [10] Brühwiler E, Bastien Masse M. Strengthening the Chillon viaducts deck slabs with reinforced UHPFRC. In: *Structural engineering: providing solutions to global challenges*. Geneva: IABSE; 2015; pp. 1171–1178.
- [11] Haber ZB, Munoz JF, De la Varga I, Graybeal BA. Bond characterization of UHPC overlays for concrete bridge decks: laboratory and field testing. *Constr Build Mater*. 2018;190:1056–1068.
- [12] Jaffrelot S. New UHPFRC deck slab for the Grand Pont in Thouaré-sur-Loire (France): How to extend the life of a 19th century metallic structure bridge? International Conference on Ultra-High Performance Fiber Reinforced Concrete, Paris, 2017, p. 807–14.
- [13] Moreillon L, Broquet C, Guillaume F, Ph M. Réfection du viaduc de Riddes. *Tracés*. 2022;3518.
- [14] SIA. *SIA 269 Bases pour la maintenance des structures porteuses*. Zurich: Société suisse des ingénieurs et des architectes; 2011.
- [15] SIA. *SIA 2052 Béton fibré ultra-performant (BFUP) – Matériaux, dimensionnement et exécution*. Zurich: Société suisse des ingénieurs et des architectes; 2016.
- [16] Moreillon L, Menétrey Ph. Rehabilitation and strengthening of existing RC structures with UHPFRC: various applications. RILEM-fib-AFGC international symposium on ultra-high performance fibre-reinforced concrete, vol. 127, Marseille, France; 2013, p. 136.
- [17] ANSYS. Inc. Ansys Mechanical. 2021 R2. 2021.
- [18] Jayaseelan H, Russell BW. *Prestress losses and the estimation of long-term deflections and camber for prestressed concrete bridges*. Stillwater: Oklahoma State University; 2007.
- [19] Ph M, Willam KJ. Triaxial failure criterion for concrete and its generalization. *ACI Struct J*. 1995; 92:311–318.
- [20] fib. *Model code for concrete structures 2010*. Lausanne: Ernst & Sohn; 2013.
- [21] Schreppers GJ, Frissen C, Kang HJ. *Prediction of crack-width and crack-pattern*. Delft, Netherlands: TNO DIANA BV, 2011.
- [22] SIA. *SIA 260 Bases pour l'élaboration des projets de structures porteuses*. Zurich: Société suisse des ingénieurs et des architectes; 2013.